ФИЗИКА ЭЛЕМЕНТАРНЫХ ЧАСТИЦ И АТОМНОГО ЯДРА
2004. Т. 35. ВЫП. 5

УДК 539.172.3

PHOTOPRODUCTION AT HERA

J. Chwastowski, J. Figiel

H. Niewodniczański Institute of Nuclear Physics,
Polish Academy of Sciences, Cracow, Poland

ФИЗИКА ЭЛЕМЕНТАРНЫХ ЧАСТИЦ И АТОМНОГО ЯДРА
2004. Т. 35. ВЫП. 5

УДК 539.172.3

PHOTOPRODUCTION AT HERA

J. Chwastowski, J. Figiel

H. Niewodniczański Institute of Nuclear Physics,
Polish Academy of Sciences, Cracow, Poland

Selected aspects of photoproduction in ep scattering at the HERA collider, studied with the ZEUS detector, are presented. The results are interpreted in the formalism of Vector Dominance Model, Regge theory, and perturbative Quantum Chromodynamics.

Представлены некоторые аспекты процессов фоторождения при электрон-протонном рассеянии на коллайдере HERA, изученные на детекторе ZEUS. Дана интерпретация результатов в формализме модели векторной доминантности, теории Редже и теории возмущений квантовой хромодинамики.

INTRODUCTION

Experiments show that photoproduction on nucleons has features similar to hadron–hadron collisions [1]. The energy dependence of the total cross section resembles that of hadron–nucleon scattering (see Fig. 1). For low energies a complicated structure corresponding to the formation of excited states or resonances is observed. Above about 3 GeV the cross section initially decreases and for larger centre-of-mass energies it increases slowly with energy. The Compton scattering, $\gamma p \to \gamma p$, shows a forward diffraction peak [2] (see Fig. 2), and its amplitude is predominantly imaginary [4]. As can be seen from Fig. 2 the elastic cross section, $d\sigma/dt$, for the three reactions: $\pi^- p \to \pi^- p$, $\gamma p \to \rho^0 p$, and $\gamma p \to \gamma p$, follows a similar behaviour with comparable values of the nuclear slope parameter, b. A copious production of the neutral vector mesons is one of the most striking features of the photoproduction.

In the first approximation a photon is an object with point-like interaction. However, it can quantum-mechanically fluctuate into a fermion–antifermion pair. The photon fluctuations into a pair of virtual charged leptons is described by QED. The photon can also fluctuate into a $q\bar{q}$ state with the photon quantum numbers ($J^{\mathrm{PC}} = 1^{--}, Q = S = B = 0$). The interaction between the $q\bar{q}$ pair and the proton will occur if the fluctuation time [5], t_f, is large compared to the interaction time, t_i. From the uncertainty principle the fluctuation time is given by

$$t_f = \frac{2E_\gamma}{m^2_{q\bar{q}}},$$

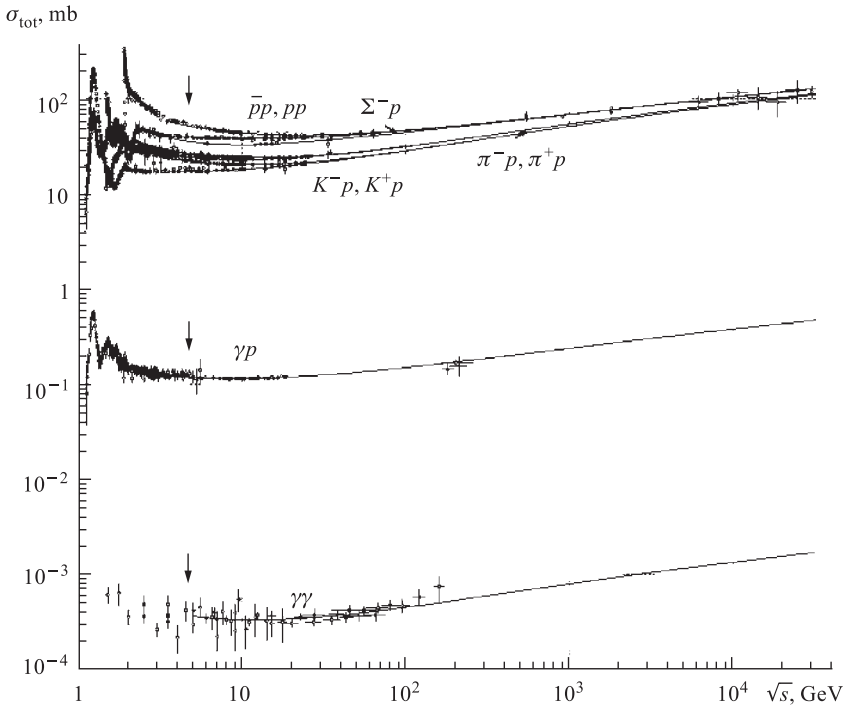

Fig. 1. Comparison of the hadronic, γp and $\gamma\gamma$ total cross sections as a function of the centre-of-mass energy (from [3])

where E_γ is the photon energy in the proton rest frame and $m_{q\bar{q}}$ is the mass of the $q\bar{q}$ state. The interaction time is of the order of the proton radius $t_i \approx 1$ fm. For interactions of 10 GeV photons with a proton at rest, assuming that the $q\bar{q}$ pair is the ρ meson, $t_f \approx 7$ fm, so the condition $t_f \gg t_i$ holds. For a virtual photon the fluctuation time is

$$t_f = \frac{2E_\gamma}{m_{q\bar{q}}^2 + Q^2},$$

where Q^2 is the photon virtuality. As Q^2 increases, the fluctuation time gets smaller (for fixed $m_{q\bar{q}}$) and the photon behaves more like a point-like object. The above picture can be used for the photon–proton scattering subprocess classification [6]. The scale of $q\bar{q}$ fluctuations can be characterized by the transverse momentum p_T of the $q\bar{q}$ system with respect to the photon direction. Small scales result in long lived fluctuations, for which there is enough time to develop a gluon cloud around the $q\bar{q}$ pair. This is the domain of the nonperturbative QCD

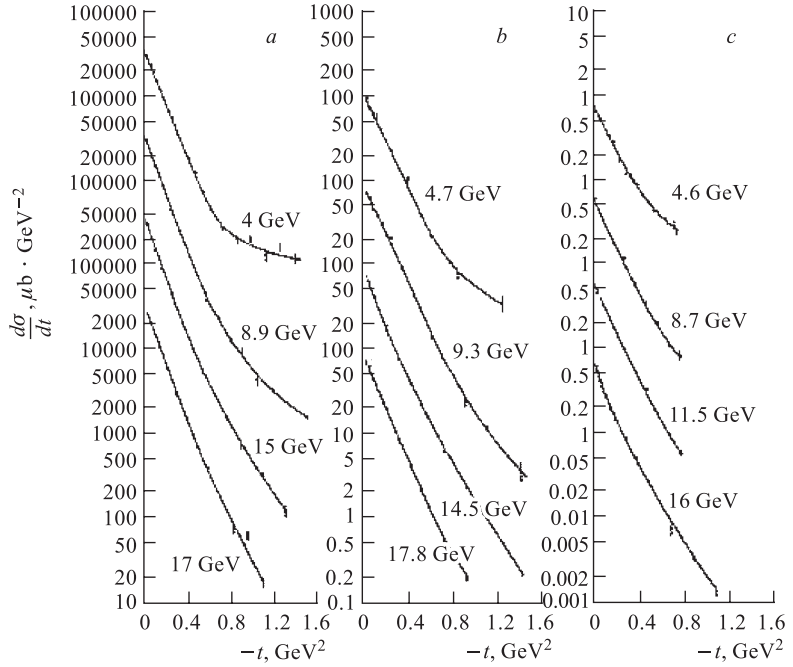

Fig. 2. Comparison of the elastic cross section $d\sigma/dt$ for the three reactions: *a*) $\pi^- p \to \pi^- p$; *b*) $\gamma p \to \rho^0 p$; *c*) $\gamma p \to \gamma p$ (from [2])

physics. Usually photoproduction of such pairs is described by a sum of over low mass vector states (the vector meson dominance model — VDM [7]). The high-p_T part should be perturbatively calculable. Summarizing, the photon can have three states: the «point-like» photon, the vector meson state and the perturbative $q\bar{q}$ pair*. This leads to three classes for γp interactions:

• the VDM class: a photon turns into a vector meson which subsequently interacts with the proton. This class contains all event types known from hadron induced reactions: an elastic and diffractive scattering, a low- and high-P_T non-diffractive interactions;

• the direct class: a photon undergoes a point-like interaction with a parton from the proton;

• the anomalous class: a photon perturbatively branches into a $q\bar{q}$ state and one of its partons interacts with a parton from the proton.

*In the following the fluctuations into the charged lepton pair are neglected.

Experimentally the high-p_T nondiffractive interaction of the VDM class and the anomalous processes are joined into the resolved processes.

1. EXPERIMENTAL ENVIRONMENT

The HERA ep storage ring [8] is well suited to study the photoproduction at high energies. The energy of the electron or positron beam is 27.5 GeV. The proton beam energy was increased to 920 from 820 GeV in 1998.

The results presented in the following were obtained by the ZEUS collaboration. The collaboration operates a general purpose magnetic detector [9]. Charged particles are tracked in the central tracking detector (CTD) [10] which operates in a magnetic field of 1.43 T provided by a thin superconducting solenoid. The high-resolution uranium-scintillator calorimeter [11] (CAL) covers 99.7% of the solid angle. It consists of three parts: the forward (FCAL), the barrel (BCAL) and the rear (RCAL) calorimeters. Each CAL part is longitudinally segmented into electromagnetic and hadronic sections. Each section is further subdivided transversely into cells. Its relative energy resolution for electromagnetic showers is $0.18/\sqrt{E(\mathrm{GeV})} \oplus 0.01$ and for hadronic showers it is $0.35/\sqrt{E(\mathrm{GeV})} \oplus 0.02$ under test-beam conditions. The HERA luminosity is measured via the rate of bremsstrahlung photons from the Bethe–Heitler process emitted at angles $\Theta_\gamma \leqslant 0.5$ mrad. The photons are registered in a lead/scintillator sandwich calorimeter [12]. It is screened from the synchrotron radiation by a carbon filter. The resulting relative energy resolution is about $0.23/\sqrt{E(\mathrm{GeV})}$. A typical systematic uncertainty on the luminosity measurement is 1–2%.

A system of electron taggers consists of three calorimeters placed at 8, 35, and 44 m away from the nominal interaction point. They tag scattered electrons in a wide energy range. In addition the lead/scintillator sandwich calorimeter placed at 35 m is used to measure the scattered electron energy. Its relative energy resolution is about $0.20/\sqrt{E(\mathrm{GeV})}$. The scattered electron energy range registered by this device is $5 \lesssim E'_e \lesssim 20$ GeV.

In fixed target experiments the photoproduction was studied by observing events induced by real photons. The photons were produced in the Bethe–Heitler process occurring when an electron passed a radiator. The measurement of the final state electron yielded the photon energy. At HERA, the electron beam is a source of quasi-real photons and the photoproduction events are divided into two classes. In the first one, «tagged events» class, the final state electron is measured in the electron taggers. For such events the photon virtuality, Q^2, is restricted to $Q_0^2 < Q^2 < 0.02$ GeV^2, where $Q_0^2 = m_e^2 y^2/(1-y)$ is the minimum value of Q^2 at a fixed value of the electron inelasticity y. The «untagged events» sample is defined requesting that the final state electron is not observed in the CAL. This requirement limits the photon virtuality to $Q^2 < 4$ GeV^2 with the median $Q^2 \approx 5 \cdot 10^{-5}$ GeV^2.

2. PHOTOPRODUCTION TOTAL CROSS SECTION

The photon–proton total cross section was measured [13] in the process $e^+p \to e^+\gamma p \to e^+X$ with the ZEUS detector at HERA. The measurement was carried out for photons with virtuality $Q^2 < 0.02$ GeV^2 and at the average photon–proton centre-of-mass energy $W_{\gamma p} = 209$ GeV. The data were collected in a dedicated run, to control systematic effects, with an integrated luminosity of 49 nb^{-1}. The measured cross section is $\sigma_{\rm tot}^{\gamma p} = 174 \pm 1(\text{stat.}) \pm 13(\text{syst.})$. The total photoproduction cross section as a function of the energy is shown in Fig. 3. The ZEUS result is in good agreement with H1 measurement [14] at a similar centre-of-mass energy. Also the low energy data are shown in the figure. In addition the ZEUS collaboration extrapolated the measurements [15] at low Q^2, $0.11 < Q^2 < 0.65$ GeV^2, to $Q^2 = 0$ using generalized VDM [16]. The extrapolation yielded $\sigma_{\rm tot}^{\gamma p} = 187 \pm 5(\text{stat.}) \pm 14(\text{syst.})$ μb at $W_{\gamma p} = 212$ GeV, a value which is somewhat larger but compatible with the direct measurement within errors. A Regge theory [17] (see also [18]) motivating the fit of the cross-section energy dependence

$$\sigma_{\rm tot}^{\gamma p} = A \cdot W_{\gamma p}^{2\epsilon} + B \cdot W_{\gamma p}^{2\eta},$$

similar to the one postulated in [19] or [20], is shown in Fig. 3 as a solid line. The first term related to the pomeron intercept as $\alpha_{I\!P}(0) = 1 + \epsilon$ describes the

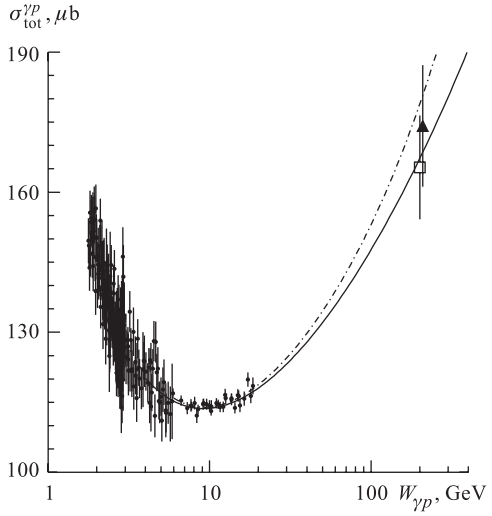

Fig. 3. The photoproduction total cross section as a function of the energy. ZEUS measurement (solid triangle), low energy data (solid circles), H1 measurement (open square), the DL98 parameterization (dash-dotted line) and the ZEUS fit (solid line) (from [13])

high-energy behaviour of the cross section. The second term corresponds to the Reggeon exchange with the intercept $\alpha_{I\!R}(0) = 1 - \eta$. The fit was performed to all the γp data [21] with $W_{\gamma p} > 4$ GeV with Reggeon intercept fixed to the value obtained by Cuddel et al. [20] $\eta = 0.358 \pm 0.015$. The fit yielded

$$A = 57 \pm 5 \ \mu\mathrm{b}, \quad B = 121 \pm 13 \ \mu\mathrm{b},$$

and

$$\epsilon = 0.100 \pm 0.012.$$

The resulting value of ϵ is in good agreement with $\epsilon = 0.093 \pm 0.002$ obtained in [20] from the analysis of hadronic data.

The Donnachie–Landshoff parameterization [19], shown as a dash-dotted line in Fig. 3, includes soft- and hard-pomeron trajectories. It agrees with the ZEUS measurement within the errors. Also other parameterizations [22–24] reproduce the ZEUS result. In addition, the total $\gamma\gamma$ cross section calculated from the assumption of the cross-section factorization

$$\sigma_{\mathrm{tot}}^{\gamma\gamma} \cdot \sigma_{\mathrm{tot}}^{pp} = (\sigma_{\mathrm{tot}}^{\gamma p})^2$$

agrees well with LEP measurements [25, 26].

3. ELASTIC VECTOR MESON PRODUCTION

An elastic vector meson production is the process

$$\gamma p \to V p,$$

where V denotes one of the vector mesons. This reaction which was extensively studied with real and virtual photons for the photon–proton centre-of-mass energy, W, below 20 GeV, exhibits features which are also characteristic for hadronic diffractive reactions. The cross-section energy dependence is weak and the dependence on t, the square of the four-momentum transfer at the proton vertex, is approximately exponential, i.e., $d\sigma/dt \sim \mathrm{e}^{-b|t|}$. This similarity can be explained on the grounds of the VDM where the photon fluctuates into a long lived vector meson state and subsequently scatters on the proton. The Regge theory predicts that at high energies the centre-of-mass energy dependence of the cross section for ρ, ω, and ϕ production is

$$\sigma_{\gamma p \to V p} \approx \frac{W^{\delta}}{b(W)}.$$

The energy dependence of the cross sections for elastic vector meson production is shown in Fig. 4 together with the HERA measurements [28–31]. Also the data

on the total photoproduction cross section are presented. The total cross section and that for the production of the lowest lying vector mesons show a similar dependence with $\delta \approx 0.22$.

For a linear pomeron trajectory the Regge prediction for the slope parameter, $b(W)$, is

$$b(W) = b_0 + 2\alpha'_{I\!P} \ln \frac{W^2}{W_0^2},$$

where $\alpha'_{I\!P}$ is the pomeron trajectory slope and b_0 and W_0 are constants. Figure 5 shows a compilation of the HERA [28, 31, 32] and low energy data [33] on the slope, b, in the case of the elastic reaction $\gamma p \to \rho p$. The Regge predictions are also depicted. The value of b rises with increasing W suggesting the shrinkage of the t-distribution forward peak with energy. The growth of b with the photon–proton centre-of-mass energy is compatible with the Regge prediction. The ZEUS collaboration finds $\alpha'_{I\!P} = 0.23 \pm 0.15(\text{stat.})^{+0.10}_{-0.07}(\text{syst.})$ GeV^{-2} consistent with the value of 0.25 GeV^{-2} obtained [27] from hadron–hadron elastic scattering.

The photoproduction of J/ψ was measured [35–37] at HERA and is shown in Fig. 4. The J/ψ photoproduction cross section has much stronger energy

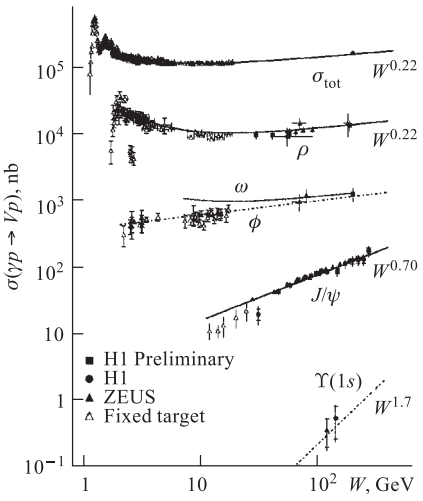

Fig. 4. The photoproduction total cross section and the cross sections for elastic vector meson production (ρ, ω, ϕ J/ψ and Υ) as a function of W. Lines show a W^δ dependence with δ values indicated (from [34])

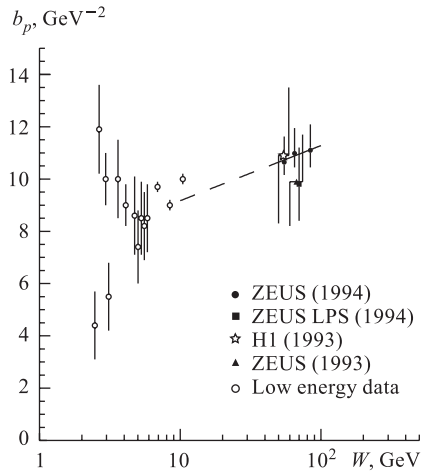

Fig. 5. Compilation of the low energy [33] and HERA [28,31,32] results on the exponential slope parameter, b, for the elastic reaction $\gamma p \to \rho p$. The solid line represents the fit of the energy dependence. The extrapolation of the fit to lower energies is marked by the dashed line (from [28])

dependence with power $\delta \approx 0.7$. This behaviour can be explained by the perturbative QCD in which the pomeron is interpreted as a two-gluon colour singlet exchange. In pQCD the steep increase of the cross section is connected [38] with the rise of the gluon density in the proton with decreasing x (increasing W). The perturbative QCD states that the cross section is proportional to the square of the gluon density function of the proton, i.e.,

$$\sigma \sim [\hat{x} g(\hat{x}, \hat{q}^2)]^2$$

with $\hat{q}^2 = (Q^2 + m^2_{J/\Psi} + |t|)/4$ and $\hat{x} = (Q^2 + m^2_{J/\Psi} + |t|)/W^2$. The mass of the J/ψ meson provides a scale large enough, $\hat{q}^2 \simeq 2.5$ GeV^2, for the perturbative QCD calculations to be valid.

Both HERA collaborations extracted the effective pomeron trajectory from the energy dependence of the slope parameter. The fitted pomeron trajectories are compatible within the errors and H1 measures [36] $\alpha_{I\!P}(0) = (1.20 \pm 0.02)$, $\alpha'_{I\!P} = (0.15 \pm 0.06)$ GeV^{-2}, while ZEUS [37] $\alpha_{I\!P}(0) = (1.200 \pm 0.009)$, $\alpha'_{I\!P} = (0.115 \pm 0.018(\text{stat.})^{+0.008}_{-0.015}(\text{syst.}))$ GeV^{-2} in a similar kinematic range. The soft-pomeron trajectory $\alpha_{I\!P}(t) = 1.08 + 0.25\,|t|$ is inconsistent with the above findings.

Measurements of the decay angular distribution of vector mesons photoproduced at small four-momentum transfer show that they have the same helicity as the interacting photon. This fact is called the s-channel helicity conservation (SCHC) and is typical for soft diffractive processes.

The elastic photoproduction of the Υ meson was measured [35, 39] via its decay into a $\mu^+\mu^-$ pair. No distinction for Υ, Υ', and Υ'' was made due to the limited experimental resolution. The cross section is small and below 1 nb (see Fig. 4). The Υ photoproduction cross section was found to be reasonably well described by the pQCD calculations. These calculations are either based on the leading vector meson cross section including corrections [40] or use the parton hadron duality hypothesis to obtain the production of Υ from the $b\bar{b}$ cross sections [41].

4. PROTON-DISSOCIATIVE VECTOR MESON PRODUCTION

The ZEUS collaboration measured the proton-dissociative (double diffractive) photoproduction of the vector mesons:

$$\gamma p \to VY,$$

where Y denotes the system in which the proton dissociates diffractively. The trigger conditions and the selection cuts ensured presence of a large rapidity gap ($\Delta\eta > 2$) between the vector meson and the system Y. The variable η is the pseudorapidity of a particle defined as $\eta = 0.5 \log(\tan(\Theta/2))$, where Θ is the

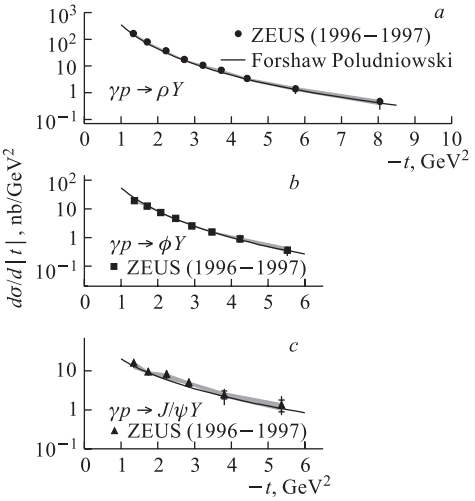

Fig. 6. The t distributions for ρ, ϕ, and J/ψ mesons in proton-dissociative photoproduction. The shaded bands represent uncertainties due to the modeling of the hadronic system Y and the lines — the pQCD calculations described in the text (from [59])

particle polar angle measured with respect to the proton direction. The production of ρ, ϕ, and J/ψ mesons, in a large $|t|$ range: $1.2 < |t| < 10$ GeV^2, at the photon–proton centre-of-mass energy $80 < W < 120$ GeV and $Q^2 < 0.02$ GeV^2 was studied [59]. In contrast to the elastic vector meson production and in accord with perturbative QCD expectation the differential cross section follows a power law dependence $|t|^{-n}$, the heavier the meson the softer the distribution: $n = 3.21 \pm 0.04 \pm 0.15$ for ρ, $n = 2.7 \pm 0.1 \pm 0.2$ for ϕ, and $n = 1.7 \pm 0.2 \pm 0.2$ for J/ψ. These data were successfully described by the pQCD calculations in [60]. The comparison of the data and calculations is depicted in Fig. 6. In this model, the virtual photon fluctuates into a $q\bar{q}$ dipole which couples via a gluon ladder (the BFKL pomeron) to a single parton ($\approx$ gluon) in the proton and then recombines into a vector meson. A nonrelativistic approximation of the vector meson wave function was used (which is very approximate in the case of light mesons). With three parameters fitted to the data, this model reproduces nicely both the shapes and the normalization for the three vector mesons. On the other hand, the two-gluon exchange failed to describe these data. Additionally, the two-gluon exchange predicts an energy independent cross section, contrary to the BFKL pomeron exchange, which foresees its rise [63]. The recent results on J/ψ photoproduction at large t obtained by the H1 collaboration [65] support this expectation and indicate the BFKL nature of the QCD pomeron in these processes.

The simultaneous measurement of the W and t dependence allowed a determination of the pomeron trajectory slope: $\alpha' = -0.02 \pm 0.05(\text{stat.})^{+0.04}_{-0.08}(\text{syst.})$ and $\alpha' = -0.06 \pm 0.12(\text{stat.})^{+0.05}_{-0.09}(\text{syst.})$ for the ρ and ϕ meson, respectively. These values are in agreement with the pQCD expectations [61] and are smaller than $\alpha' = 0.25$ GeV^{-2} characteristic for soft processes at $-t < 0.5$ GeV^2 and also than those measured for $-t < 1.5$ GeV^2 [62]. These observations establish $|t|$ as a hard pQCD scale similarly to Q^2 in DIS. More quantitative comparison can be obtained by plotting the ratios of vector meson cross sections in the function of both scales, Q^2 and $|t|$ [59]. Under simplifying assumptions that the photon couples directly to quarks in the vector meson and that the coupling does not depend neither on the vector meson mass nor on its wave function (which seems reasonable in a hard scattering) these ratios reach $SU(4)$ values of 2/9 for ϕ/ρ and 8/9 for $J/\Psi/\rho$. In fact the ϕ/ρ ratios approach the $SU(4)$ values with increasing Q^2 and $|t|$, as well as Ψ/ρ in the photoproduction ($|t|$). Generally, however the cross-section ratios rise faster with increasing $|t|$ than with Q^2, so these scales seem not to be equivalent.

The analysis of the angular distributions of the meson decay products was used to determine the ρ and ϕ spin-density matrix elements [59]. They are r^{04}_{00} and r^{04}_{10} related to the single helicity flip amplitudes and r^{04}_{1-1} related to the double helicity flip amplitudes. Following the pQCD predictions and contrary to soft diffractive processes in which the helicity is conserved (SCHC hypothesis), all these matrix elements are significantly different from zero: r^{04}_{00} and $\text{Re}\,(r^{04}_{10}) \approx 0.05$ and $r^{04}_{1-1} \approx -0.15$ in the whole $|t|$-range considered [59]. These observations are semiquantitatively reproduced in the BFKL framework [64].

5. INCLUSIVE DIFFRACTION

A photon can dissociate not only into vector mesons but also into a multiparticle hadronic state (X), of mass M_X in the process of inclusive diffraction:

$$\gamma p \to X p$$

if the coherence condition $M_X^2/W^2 \ll 1$ is satisfied. The E-612 experiment at Fermilab studied this reaction in the scattering of real photons off protons in the kinematic range $75 < E_\gamma < 148$ GeV, $0.02 < |t| < 0.1$ GeV^2 and $M_X^2/W^2 < 0.1$. At low mass it was found that the cross section is dominated by the ρ production. The t distribution in the ρ mass region is exponential with a slope parameter $b = 10.6 \pm 1.0$ GeV^{-2}. For larger masses the slope of the t distribution is roughly half of that for the ρ region. At high values of M_X^2 a dominant $1/M_X^2$ behaviour was observed. The diffractive events were characterized by the lack of the hadronic activity between the photon system X

and the final proton. This topological feature of the diffractive final state is called Large Rapidity Gap (LRG).

Photon inclusive diffractive dissociation was studied by H1 [43] and ZEUS [44] collaborations using the LRG signature. Experimentally, the events were selected requiring a pseudorapidity gap $\Delta\eta$ between the most forward hadron (of pseudorapidity $\eta_{\max}$) and the final proton. The H1 collaboration carried out measurements at $W = 187$ and 231 GeV. They found that the energy and M_X^2 dependence of the H1 data and of the low energy data [42] is well described by the triple-Regge mechanism. The extracted effective intercept of the pomeron trajectory is $\alpha_{I\!P}(0) = 1.068 \pm 0.016(\text{stat.}) \pm 0.022(\text{syst.}) \pm 0.041(\text{model})$ and agrees well with the one obtained for hadron–hadron scattering.

The ZEUS collaboration performed a study of the M_X^2 distribution at $W \approx 200$ GeV and found that for large masses ($8 < M_X^2 < 24$ GeV^2) the triple-Regge mechanism provides a good description of the data. The analysis yielded a value of the effective intercept of the pomeron trajectory $\alpha_{I\!P}(0) = 1.12 \pm 0.04(\text{stat.}) \pm 0.07(\text{syst.})$ which is consistent with the one found by H1 within the errors. The ZEUS collaboration found also that the ratio of the cross section for the photon diffractive dissociation to the total photoproduction cross section is $(13.3 \pm 0.5(\text{stat.}) \pm 3.6(\text{syst.}))\%$.

In photoproduction the LRG signature is also observed in events with production of jets. The large rapidity gap can be between the jets and the target particle as proposed in the Ingelman–Schlein model [45]. In this case the four-momentum transfer is small and the target particle preserves its identity. Bjorken [46] proposed to study the events in which the gap separates the jets. In such events the four-momentum transfer is large.

Both ZEUS and H1 analyzed events with the production of jets and a LRG in the proton fragmentation region [47,48]. Figure 7 shows the $\eta_{\max}$ distribution

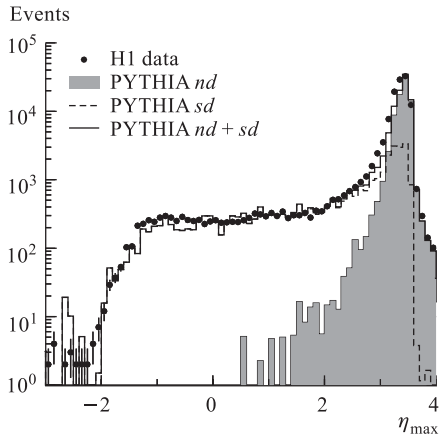

Fig. 7. The $\eta_{\max}$ distribution for photoproduction events containing jets of $E_T > 5$ GeV and $-1.5 < \eta_{\text{jet}} < 2.5$ compared to the PYTHIA MC predictions. The nondiffractive PYTHIA version is depicted by the shaded histogram, the diffractive one is marked by the dashed line, and a sum of both, by the solid line (from [48])

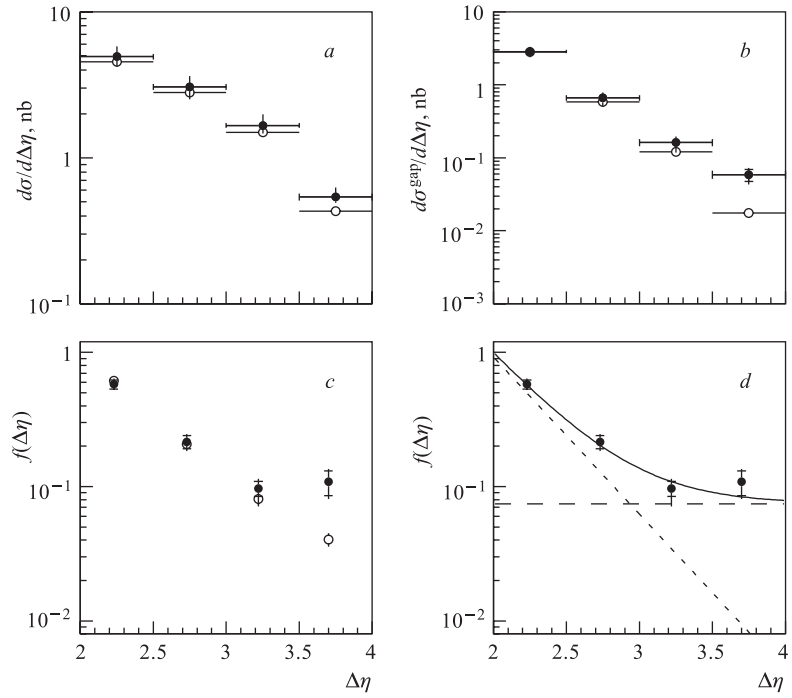

Fig. 8. Inclusive cross section, $d\sigma/d\Delta\eta$, as a function of the pseudorapidity distance $\Delta\eta$ between the jets (a) and for events with the LRG signature (b). ZEUS data — black circles. The PYTHIA prediction for a nonsinglet exchange — open circles. The gap fraction as a function of $\Delta\eta$ is depicted in c and d where also the result of the fit (solid line) to a sum of an exponential and a constant (dotted lines) is shown (from [53])

for such events. A clear excess of data over the nondiffractive Monte Carlo is observed for $\eta_{\max} < 2$. The sum of the nondiffractive and diffractive PYTHIA MC [49] well describes the data.

The ZEUS collaboration estimated in [47] that the gluon content of the pomeron should be 30–80% to describe the data with the help of the Ingelman–Schlein model. The measured cross sections for the diffractive dijet photoproduction [50,51] show a steep fall-off with the transverse jet energy, $E_T^{\rm jet}$, as expected for parton–parton scattering. Recently, the H1 collaboration published an analysis [52] of the diffractively produced jets in tagged photoproduction. They found that the Monte Carlo prediction, based on the H1 2002 QCD fit, well describes the shapes of the differential cross sections. However, the normalization is overestimated by a factor of about 1.3. The shape of the differential cross section is well represented if in the Monte Carlo model the pomeron intercept of $\alpha_{I\!P}(0) = 1.17$ or $\alpha_{I\!P}(0) = 1.08$ is used, while the choice of $\alpha_{I\!P}(0) = 1.4$ is disfavoured.

Events with large rapidity gap between the jets were studied by the ZEUS [53] and H1 [54] collaborations. Such events can be due to the exchange of a colour singlet object. The exchange of an electroweak boson or a strongly interacting colour singlet is possible. These exchanges would lead to similar results however their rates can be different. If the jets have large transverse energies, then the four-momentum transfer is large and the process can be perturbatively calculated. Bjorken [46] estimated that the ratio of the colour singlet two-gluon exchange to the single gluon exchange is about 0.1.

For events containing two jets the gap fraction, $f(\Delta\eta)$, is defined as a number of dijet events with a certain gap size $\Delta\eta$ to the total number of dijet events for which the distance between the jets is $\Delta\eta$. The ZEUS collaboration used events with at least two jets of $E_T > 6$ GeV and separated in pseudorapidity by at least 2 units. The region between the jet cones with no particle of the transverse energy, $E_T^{\rm part} > 250$ MeV, is called a gap. The data and the PYTHIA MC predictions are compared in Fig. 8. A clear excess of events for large values of $\Delta\eta$ is observed. The gap fraction for the colour singlet is found to be about $0.07 \pm 0.02^{+0.01}_{-0.02}$. It is larger than the values measured at Tevatron ~ 0.01 [55,56]. The H1 collaboration used events with at least two jets with transverse energies $E_T^{\rm jet1} > 6$ GeV and $E_T^{\rm jet2} > 5$ GeV and separated by at least 2.5 pseudorapidity units. In addition, H1 measures the total activity between the jets as $E_T^{\rm gap}$ which is the sum of the transverse energies observed in the region between two highest E_T jets. For the lowest value of $E_T^{\rm gap} < 0.5$ GeV and $3.5 < \Delta\eta < 4.0$ the gap fraction is approximately 10% in good agreement with the ZEUS result.

6. HARD JETS IN PHOTOPRODUCTION

The photoproduction of jets at a large scale provided by the transverse energy, E_T, of jets can be computed in perturbative QCD. Examples of the leading order QCD (LO QCD) diagrams for inclusive jet production are shown in Fig. 9. In LO QCD, such processes are divided into two classes. In the first one, called resolved process, the photon acts as a source of partons and only a fraction of its momentum, x_γ, participates in the scattering. In the second one, the direct process, the photon interacts via boson-gluon fusion or QCD Compton scattering and acts as a point-like particle with $x_\gamma \approx 1$. Both classes lead to the production of jets. However, they differ in the jet topology. The resolved events contain the so-called photon remnant jet (see Fig. 9). Jet cross sections are sensitive to the photon and the proton structures and to the dynamics of the hard subprocess. For high E_T values the influence of less-well understood soft processes is reduced.

The jet photon–proton cross section, $d\sigma_{\gamma p}$, can be written as

$$d\sigma_{\gamma p} = \sum_{ab} \int_{x_\gamma} \int_{x_p} dx_p dx_\gamma f_p(x_p, \mu^2) f_\gamma(x_\gamma, \mu^2) d\hat{\sigma}_{ab}(x_p, x_\gamma, \mu^2)(1 + \delta_{\rm hadr}),$$

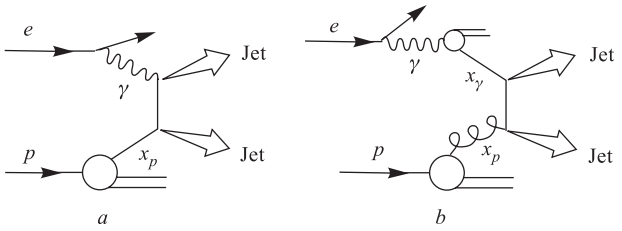

Fig. 9. Examples of the LO QCD diagrams for inclusive jet photoproduction in direct (a) and resolved (b) processes

where f_p is the proton–parton density function (PDF); f_γ is the photon PDF; $\hat{\sigma}_{ab}$ describes the hard partonic cross section; μ represents both the factorization and renormalization scales; x_γ is the fraction of the photon's energy participating in the generation of jets and x_p is the fractional momentum at which the partons inside the proton are probed. The hadronization correction, $\delta_{\rm hadr}$, takes into account nonperturbative effects. It can be estimated using Monte Carlo models for the parton cascade and fragmentation. For the direct component the photon PDF reduces to the Dirac δ function at $x_\gamma = 1$. The cross sections for the inclusive jet photoproduction were measured by the H1 [66] and ZEUS [67] collaborations. The ZEUS measurement is presented in Fig. 10. The LO QCD calculations fail

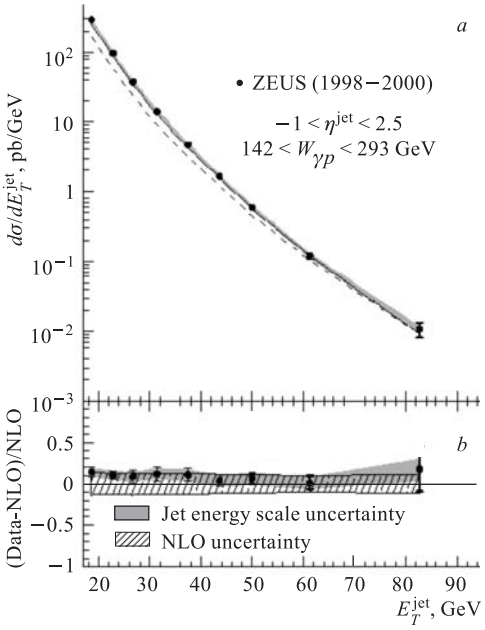

Fig. 10. a) Measured inclusive jet cross section, $d\sigma/dE_T^{\rm jet}$ (solid dots) compared to LO and NLO QCD calculations. The thick error bars represent the statistical uncertainties, the thin error bars show the statistical and systematic uncertainties added in quadrature. The shaded band shows the uncertainty associated to the absolute energy scale of the jets. The LO (dashed line) and NLO (solid line) QCD parton-level calculations corrected for hadronization effects are also shown. b) The fractional difference between the measured $d\sigma/dE_T^{\rm jet}$ and the NLO QCD calculation with the calculation uncertainty marked by hatched band (from [67])

to reproduce the data. The next-to-leading order QCD (NLO QCD) predictions deliver a good description of the measured distribution. It was found [66] that the cross section calculated with the GRV [68] photon PDF gives values which are 5–10% larger than those obtained with AFG [69]. Different parameterizations of the proton PDF have a small effect at low values of $E_T^{\rm jet}$. With increasing jet transverse energy differences appear, when CTEQ5M [70] based calculations are compared to those obtained with MRST99 [71] or CTEQ5HJ [70].

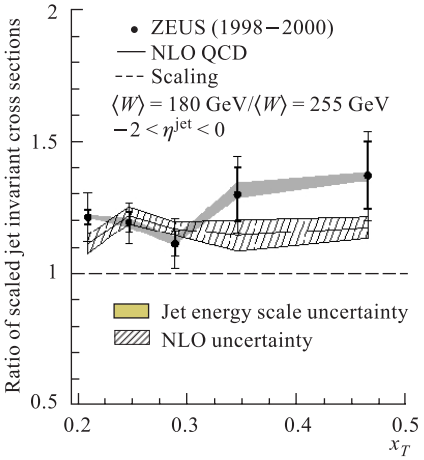

Fig. 11. Measured ratio of the scaled jet invariant cross sections at two W intervals as a function of x_T (from [67])

The ZEUS collaboration measured the scaled invariant cross section, $(E_T^{\rm jet})^4(E^{\rm jet}d^3\sigma/dp_X^{\rm jet}p_Y^{\rm jet}p_Z^{\rm jet})$, where $E_T^{\rm jet}$ is the jet tranverse energy and $E^{\rm jet}$ is the jet energy. The measurement was performed for jets with the pseudorapidity $-2 < \eta_{\gamma p}^{\rm jet} < 0$ measured in the photon–proton centre-of-mass frame at the two values of the photon–proton centre-of-mass energy $W = 180$ GeV and $W = 255$ GeV. The ratio of the scaled invariant cross sections when plotted as a function of the variable $x_T = 2E_T^{\rm jet}/W$ shows the scaling violation. This is depicted in Fig. 11. The inclusive jet cross section can be used to determine the value of the strong coupling constant, $\alpha_s(M_Z)$. The measured value

$$\alpha_s(M_Z) = 0.1224 \pm 0.0001({\rm stat.})^{+0.0022}_{-0.0019}({\rm exp.})^{+0.0054}_{-0.042}({\rm th.})$$

is consistent with the world average $\alpha_s(M_Z) = 0.1183 \pm 0.0027$ [72] (see Fig. 12, a) and the measurements [73, 74] in NC DIS and the $p\bar{p}$ interactions [75]. When plotted as a function of the jet transverse energy, α_s shows (see Figs. 12, b, c) a clear running behaviour.

For the dijet photoproduction x_γ is estimated by $x_\gamma^{\rm obs}$ which measures the fraction of the photon energy participating in the production of the two highest energy jets [76]

$$x_\gamma^{\rm obs} = \frac{E_T^{\rm jet1}\,{\rm e}^{-\eta_{\rm jet1}} + E_T^{\rm jet2}\,{\rm e}^{-\eta_{\rm jet2}}}{2yE_e},$$

where $E_T^{\rm jet1,2}$ are the transverse energies of the jets in the laboratory frame; $\eta_{\rm jet1,2}$ are the jets' pseudorapidities, and y is the fraction of the incident lepton energy carried by the photon in the proton rest frame. In the leading order QCD $x_\gamma =$

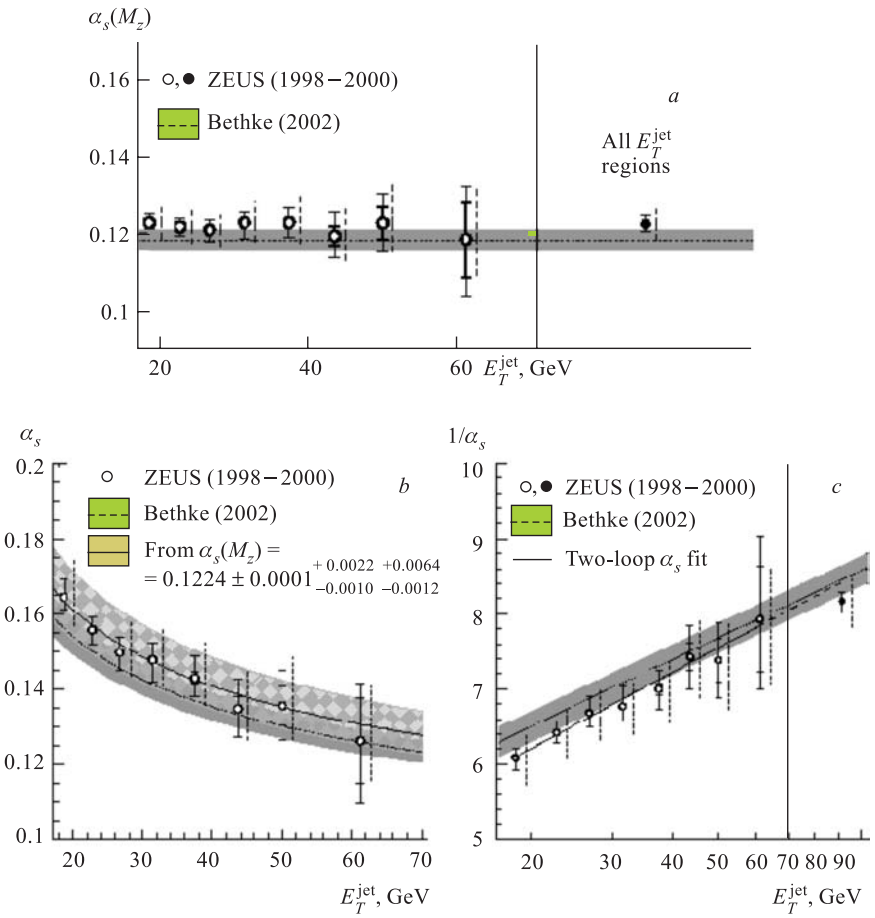

Fig. 12. *a*) The $\alpha_s(M_Z)$ values (open circles) as a function of $E_T^{\rm jet}$. The combined result using all the $E_T^{\rm jet}$ intervals is shown as a solid circle. *b*) The value $\alpha_s(E_T^{\rm jet})$ as a function of $E_T^{\rm jet}$ (open circles). The solid line represents the predictions for the central value of $\alpha_s(M_Z)$ measured by the ZEUS collaboration with the uncertainty given by the light-shaded band. *c*) The value $1/\alpha_s(E_T^{\rm jet})$ as a function of $E_T^{\rm jet}$ (open circles). The solid line represents the result of the two-loop α_s fit to the measured values. The dashed line shows the extrapolation to $E_T^{\rm jet} = M_Z$. In all figures the inner error bars show the statistical uncertainty, and outer error bars represent the statistical and systematic uncertainties added in quadrature. The dashed error bars show the theoretical uncertainties. The world average (dotted line) and its uncertainty (shaded band) are displayed (from [67])

$x_\gamma^{\rm obs}$. The distribution of $x_\gamma^{\rm obs}$ is shown in Fig. 13 together with the PYTHIA [49] and Herwig [80] Monte Carlo predictions. The resolved component dominates below $x_\gamma^{\rm obs} \approx 0.8$ while above this value the direct processes are more important [77,78].

The distribution of the angle, Θ^*, between the jets in the parton–parton c.m.s. can be used to test the dynamics of the dijet photoproduction. For two-to-two massless parton scattering

$$\cos\,\Theta^* = \tanh\left(\frac{\eta^{\rm jet1} - \eta^{\rm jet2}}{2}\right)$$

QCD predicts different dijet angular distributions for the resolved and direct components. For the latter, mediated mainly by a quark, the distribution is $d\sigma/d|\cos\,\Theta^*| \sim (1 - |\cos\,\Theta^*|)^{-2}$. If the process is mediated by a gluon exchange, like in the case of the resolved component, the distribution is $d\sigma/d|\cos\,\Theta^*| \sim (1-|\cos\,\Theta^*|)^{-1}$. The dijet photoproduction cross sections were measured [77,78] by both HERA collaborations. The ZEUS measurement [78] of $d\sigma/d|\cos\,\Theta^*|$ is presented in Fig. 14. For $x_\gamma^{\rm obs} < 0.75$, the region enriched in the resolved component, the measured cross section lies above the NLO QCD predictions using GRV-HO for the photon PDF. Given the theoretical and experimental uncertainties, the NLO calculations [81] reasonably well describe the data. The calculations using AFG-HO are below that of the GRV-HO. For $x_\gamma^{\rm obs} > 0.75$, the direct region, the NLO predictions are in agreement with the measured cross section. In Fig. 14, *c* the shapes of the data and the NLO distributions are compared. The data for $x_\gamma^{\rm obs} < 0.75$ rise more rapidly with $|\cos\,\Theta^*|$ than those in the direct component dominated region. This is consistent with a difference in the dominant propagators. A similar observation was made in [77]. The agreement between the data and the NLO QCD calculations at the high $x_\gamma^{\rm obs}$ and high transverse energy, where the dependence on the photon structure is small, show a consistency between the data and the gluon distribution in the proton extracted from DIS data. Further discrimination between the photon PDFs is difficult due to large uncertainties in the theory at low transverse energies and both the theoretical and experimental uncertainties at higher transverse energies. Further constraints of the parton densities in the photon can be made more stringent by including the higher-order or resummed calculations.

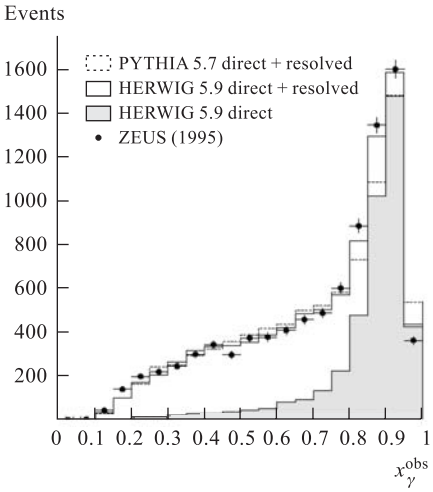

Fig. 13. The $x_\gamma^{\rm obs}$ distribution for the data [79] compared to MC predictions. The simulated distributions were fitted to the data (from [79])

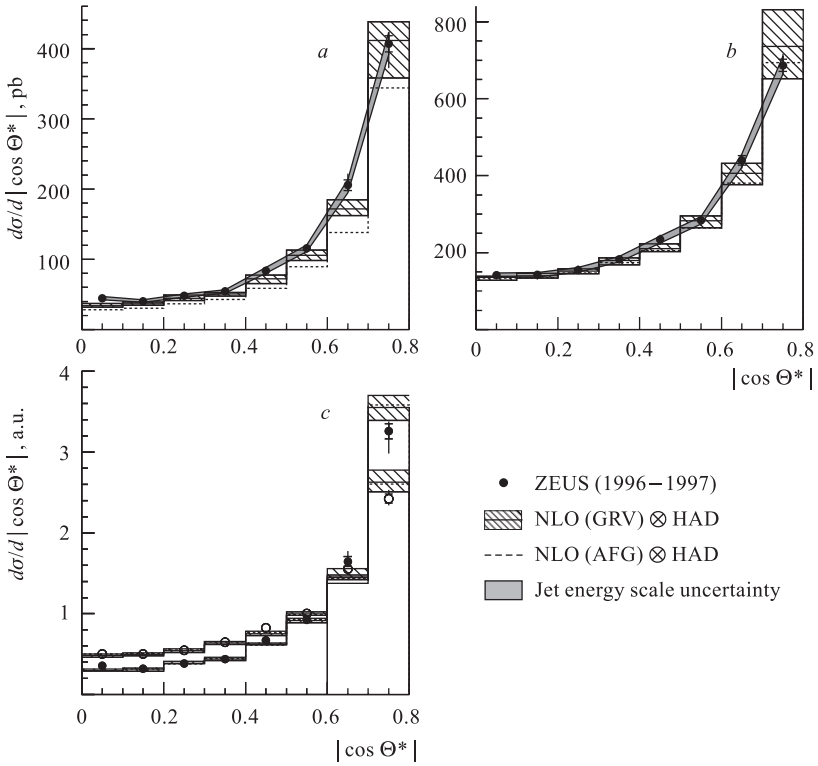

Fig. 14. Measured cross sections as a function of $|\cos\Theta^*|$ for $x_\gamma^{\rm obs} < 0.75$ (a) and $x_\gamma^{\rm obs} > 0.75$ (b) compared to NLO predictions obtained using GRV-HO and CTEQ5M1 PDFs for the photon and proton, respectively. Hatched band represents theoretical uncertainties. Shaded band shows the jet energy uncertainty. Predictions using AFG-HO are depicted as dashed line. c) The cross sections are area normalized and the data for $x_\gamma^{\rm obs} < 0.75$ (solid circles) and for $x_\gamma^{\rm obs} > 0.75$ (open circles) are shown (from [78])

7. INELASTIC PHOTOPRODUCTION OF J/ψ

The inelastic J/ψ photoproduction arises from direct or resolved photon interactions. In perturbative QCD it can be calculated in the colour-singlet (CS) and colour-octet (CO) frameworks. In the former case a colourless $c\bar{c}$ pair produced by the hard subprocess is identified with the physical J/ψ meson whereas in the latter, the $c\bar{c}$ pair is produced with nonzero colour and then emits one or more gluons becoming finally a colourless meson. The predictions of the CS model underestimate the observed J/ψ production in $p\bar{p}$ interactions by a large factor [83] and this difference can be accounted for by the CO contribution.

The ZEUS collaboration investigated [82] the inelastic charmonium (J/ψ and ψ') photoproduction in the energy range $50 < W < 180$ GeV, through their decays into muon pairs. The J/ψ production cross section as a function of its transverse momentum, p_T, and the inelasticity, z (the fraction of incoming photon's energy carried by the J/ψ) is shown in Figs. 15 and 16 and is compared with the theoretical calculations mentioned previously. A prediction of the colour-singlet model in the leading logarithms approximation (LO, CS) does not clearly describe the p_T distribution. Including next-to-leading corrections (NLO, CS) it matches the data very well suffering however from some theoretical uncertainty [84]. The same is valid for the inelasticity distribution (see Fig. 16). In this figure the predictions of two particular calculations using both singlet and octet colour mechanisms and the leading logarithms approximation (LO, CS+CO) are also presented. The NLO QCD calculations provide a prediction which is consistent with the data within large uncertainties resulting from extracting the CO matrix elements [84, 85]. These inconclusive results mean that a quantitative understanding of the J/ψ production mechanism is still lacking.

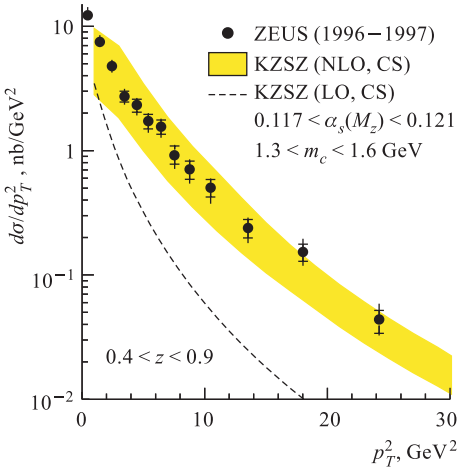

Fig. 15. The J/ψ differential cross section $d\sigma/dp_T^2$. The data are compared with two predictions of the colour-singlet model described in the text (from [82])

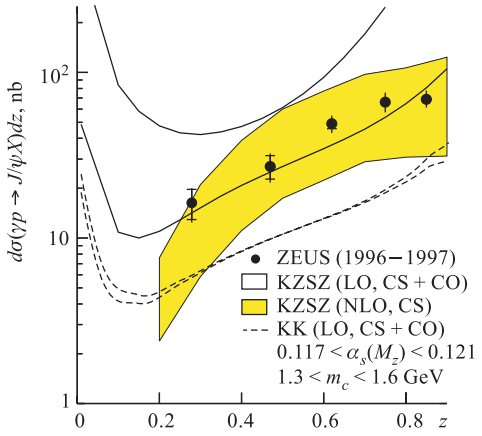

Fig. 16. The J/ψ differential cross section $d\sigma/dz$ for $p_T > 1$ GeV. The data are compared with predictions of the colour-singlet model and two predictions including both the colour-singlet and colour-octet contributions described in the text (from [82])

8. BEAUTY PHOTOPRODUCTION

Beauty photoproduction, owing to the large mass of the b quark which provides a hard scale, is a stringent test of perturbative QCD.

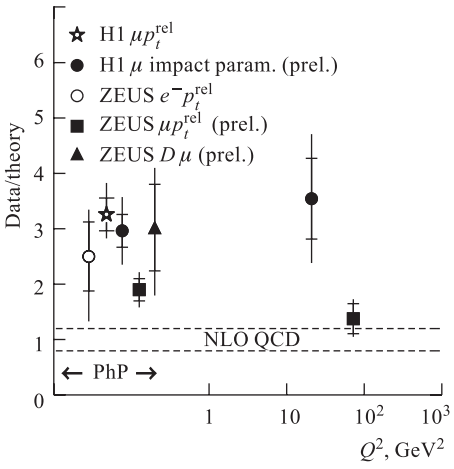

Fig. 17. Ratio of the measured b-production cross section at HERA and the theoretical expectation from NLO QCD, as a function of Q^2. A star and circles represent older H1 and ZEUS results [88]. A triangle represents the photoproduction measurement using $D^*+\mu$ tag [89] (from [86])

The ZEUS collaboration investigated [86] this process using events with two high transverse energy jets and a muon in the final state. The fraction of beauty quarks in the data was determined using the transverse momentum distribution of the muon relative to the closest jet. The total and differential cross sections for the process $ep \to b\bar{b} \to 2$ jets $+ X$ were determined using Monte Carlo models to extrapolate for the unmeasured part of the muon kinematics and to correct for the inclusive branching ratio $B(b \to \mu)$. The measured cross sections were compared to NLO QCD predictions based on the program by Frixione et al. [87]. This is summarized in Fig. 17 where the ratio of the measured to the predicted cross section is presented as a function of Q^2. For $Q^2 \sim 0$ this ratio is about 2 which demonstrates that the model considerably underestimates the beauty photoproduction. The differential cross section in the region of a good muon acceptance is also larger than the theoretical prediction however compatible with it within the experimental and theoretical uncertainties. The excess of b-quark production over NLO QCD predictions was also found in $p\bar{p}$ annihilations (see references in [86]). The above observations are a challenge for the perturbative QCD.

9. SUMMARY

Selected aspects of the photoproduction study with the ZEUS detector at HERA have been presented. The photon–proton interactions show many features similar to soft hadron–hadron collisions. However, in the presence of a large scale, delivered by the meson mass or the transverse energy, the hard scattering of partonic constituents in the photon and proton becomes important. Many partic-

ular features of the hard γp interactions are successfully described by perturbative QCD based models.

Acknowledgements. We gratefully acknowledge support of the DESY directorate during our stays at DESY. We thank our colleagues from the ZEUS collaboration for their help, co-operation and creation of a stimulating atmosphere. The authors thank Prof. E. Lohrmann for discussions and the critical reading of the manuscript.

REFERENCES

1. *Bauer T. H. et al.* // Rev. Mod. Phys. 1978. V. 50. P. 261.
2. *Kogan E.* Ph. D. Thesis. Weizmann Institute, Rehovot, Israel (unpublished); Rev. Mod. Phys. 1978. V. 50. P. 270.
3. *Hagiwara K. et al.* (*Particle Data Group*) // Phys. Rev. D. 2002. V. 66. P. 010001.
4. *Alvensleben H. et al.* // Phys. Rev. Lett. 1973. V. 30. P. 328.
5. *Ioffe B. L.* // Phys. Lett. B. 1969. V. 30. P. 123;
   Ioffe B. L., Khoze V. A., Lipatov L. N. // Hard Processes. 1984. V. 1. P. 155.
6. *Schuler G. A., Sjöstrand T.* // Nucl. Phys. B. 1993. V. 407. P. 529;
   Schuler G. A., Sjöstrand T. CERN-TH 6796/93.
7. *Sakurai J. J.* // Ann. Phys. (N. Y.). 1960. V. 11. P. 1;
   Sakurai J. J. // Phys. Rev. Lett. 1969. V. 22. P. 981.
8. A Proposal for a Large Electron–Proton Colliding Beam Facility at DESY. DESY HERA 81-10. 1981;
   Wiik B. H. Electron–Proton Colliding Beams. The Physics Programme and the Machine // Proc. of the 10th SLAC Summer Institute. 1982. P. 233.
9. *ZEUS Collab.* The ZEUS Detector. Technical Proposal. 1986; The ZEUS Detector. Status Report 1993. DESY, 1993; http://www-zeus.desy.de/bluebook/bluebook.html
10. *Foster B. et al.* // Nucl. Instr. Meth. A. 1993. V. 338. P. 254.
11. *Derrick M. et al.* // Ibid. V. 309. P. 77;
    Berstein A. et al. // Ibid. V. 336. P. 23;
    Anderson A. et al. // Ibid. V. 309. P. 101.
12. *Andruszków J. et al.* DESY 92-066. 1992;
    Andruszków J. et al. // Acta Phys. Polon. B. 2001. V. 32. P. 2025.
13. *Chekanov S. et al.* (*ZEUS Collab.*) // Nucl. Phys. B. 2002. V. 627. P. 3.
14. *Aid S. et al.* (*H1 Collab.*) // Z. Phys. C. 1995. V. 69. P. 27.
15. *Derrick M. et al.* (*ZEUS Collab.*) // Eur. Phys. J. C. 1999. V. 7. P. 609.
16. *Sakurai J. J., Schildknecht D.* // Phys. Lett. B. 1972. V. 40. P. 121.
17. *Regge T.* // Nuovo Cim. 1959. V. 14. P. 951;
    Regge T. // Nuovo Cim. 1960. V. 18. P. 947.
18. *Collins P. D. B.* An Introduction to Regge Theory and High Energy Physics. Cambridge University Press, 1977.

19. *Donnachie A., Landshoff P. V.* // Phys. Lett. B. 1998. V. 437. P. 408.
20. *Cudell J. R. et al.* // Phys. Rev. D. 2000. V. 61. P. 034019; Erratum. 2001. V. 63. P. 059901.
21. *Alekhin S. I. et al.* (*HERA and Compass Groups*). CERN-HERA-8701. 1987.
22. *Friberg C., Sjöstrand T.* // J. High Ener. Phys. 2000. V. 09. P. 10.
23. *Block M. M. et al.* // Phys. Rev. D. 1999. V. 60. P. 054024;
Block M. M., Halzen F., Stanev T. // Phys. Rev. D. 2000. V. 62. P. 077501.
24. *Abramowicz H., Levy E.* DESY-97-251.
25. *Acciarri M. et al.* (*L3 Collab.*) // Phys. Lett. B. 2001. V. 519. P. 33.
26. *Abbiendi G. et al.* (*OPAL Collab.*) // Eur. Phys. J. C. 2000. V. 14. P. 199.
27. *Donnachie A., Landshoff P. V.* // Phys. Lett. B. 1992. V. 296. P. 227.
28. *Breitweg J. et al.* (*ZEUS Collab.*) // Eur. Phys. J. C. 1998. V. 2. P. 247.
29. *Derrick M. et al.* (*ZEUS Collab.*) // Z. Phys. C. 1996. V. 73. P. 73.
30. *Derrick M. et al.* (*ZEUS Collab.*) // Phys. Lett. B. 1996. V. 377. P. 259.
31. *Aid S. et al.* (*H1 Collab.*) // Nucl. Phys. B. 1996. V. 463. P. 3.
32. *Derrick M. et al.* (*ZEUS Collab.*) // Z. Phys. C. 1995. V. 69. P. 39.
33. *Jones W. G. et al.* // Phys. Rev. Lett. 1968. V. 21. 586;
Berger C. et al. // Phys. Lett. B. 1972. V. 39. P. 659;
Ballam J. et al. (*SBT Collab.*) // Phys. Rev. D. 1972. V. 5. P. 545;
Gladding G. E. et al. // Phys. Rev. D. 1973. V. 8. P. 3721.
34. *Fleischmann P.* (*H1 Collab.*) // Proc. of DIS 2003, St. Petersburg, Russia, April 23–27, 2003 (to appear).
35. *Aldoff C. et al.* (*H1 Collab.*) // Phys. Lett. B. 2000. V. 483. P. 23.
36. *H1 Collab.* // XXI Intern. Europhysics Conf. on High Energy Physics (ESP03), Aachen, July 17–23, 2003. Abstr. 108 (submitted).
37. *Chekanov S. et al.* (*ZEUS Collab.*) // Eur. Phys. J. C. 2002. V. 24. P. 345.
38. *Ryskin M.* // Z. Phys. C. 1993. V. 57. P. 89.
39. *Breitweg J. et al.* (*ZEUS Collab.*) // Phys. Lett. B. 1998. V. 437. P. 432.
40. *Frankfurt L. , McDermott M., Strickman M.* // J. High Ener. Phys. 1999. V. 02. P. 002.
41. *Martin A. D., Ryskin M. G., Teubner T.* // Phys. Lett. B. 1999. V. 454. P. 339.
42. *Chapin T. J. et al.* // Phys. Rev. D. 1985. V. 31. P. 17.
43. *Adloff C. et al.* (*H1 Collab.*) // Z. Phys. C. 1997. V. 74. P. 221.
44. *Breitweg J. et al.* (ZEUS Collab.) // Ibid. V. 75. P. 421.
45. *Ingelmann G., Schlein P. E.* // Phys. Lett. B. 1985. V. 152. P. 256.
46. *Bjorken J. D.* // Phys. Rev. D. 1993. V. 47. P. 101.
47. *Derrick M. et al.* (*ZEUS Collab.*) // Phys. Lett. B. 1995. V. 356. P. 129.
48. *Ahmed T. et al.* (*H1 Collab.*) // Nucl. Phys. B. 1995. V. 435. P. 3.
49. *Sjöstrand T.* // Comp. Phys. Commun. 1994. V. 82. P. 74;
Sjöstrand T. PYTHIA 5.7. hep-ph-/9508391.
50. *Adloff C. et at.* (*H1 Collab.*) // Eur. Phys. J. C. 1999. V. 6. P. 421.

51. *Breitweg J. et al.* (*ZEUS Collab.*) // Eur. Phys. J. C. 1998. V. 5. P. 45.
52. *H1 Collab.* Contribution // XXI Intern. Europhysics Conf. on High Energy Physics (EPS03), Aachen, July 17–23, 2003. Abstr. 087.
53. *Derrick M. et al.* (*ZEUS Collab.*) // Phys. Lett. B. 1996. V. 369. P. 55.
54. *Adloff C. et al.* (*H1 Collab.*) // Eur. Phys. J. C. 2002. V. 24. P. 517.
55. *Abe F. et al.* (*CDF Collab.*) // Phys. Rev. Lett. 1995. V. 74. P. 855.
56. *Abachi S. et al.* (*D0 Collab.*) // Phys. Rev. Lett. 1996. V. 76. P. 734.
57. *Aldloff C. et al.* (*H1 Collab.*) // Z. Phys. C. 1997. V. 76. P. 613.
58. *Breitweg J. et al.* (*ZEUS Collab.*) // Eur. Phys. J. C. 1999. V. 6. P. 43.
59. *Chekanov S. et al.* (*ZEUS Collab.*) // Eur. Phys. J. C. 2003. V. 26. P. 389.
60. *Forshaw J. R., Poludniowski G.* // Ibid. P. 411.
61. *Bartels J. et al.* // Phys. Lett. B. 1996. V. 375. P. 301;
Ivanov D. Yu. et al. // Phys. Lett. B. 2000. V. 478. P. 101; Erratum. 2001. V. 348. P. 295.
62. *Breitweg J. et al.* (*ZEUS Collab.*) // Eur. Phys. J. C. 2000. V. 14. P. 213.
63. *Enberg R., Motyka L., Poludniowski G.* // Eur. Phys. J. C. 2003. V. 26. P. 219.
64. *Enberg R., Motyka L., Poludniowski G.* // Acta Phys. Pol. B. 2002. V. 33. P. 3511.
65. *Aktas A. et al.* (*H1 Collab.*) DESY 03-061. 2003.
66. *Adloff C. et al.* (*H1 Collab.*) // Eur. Phys. J. C. 2003. V. 29. P. 497.
67. *Chekanov S. et al.* (*ZEUS Collab.*) // Phys. Lett. B. 2003. V. 560. P. 7.
68. *Glück M., Reya E., Vogt A.* // Phys. Rev. D. 1992. V. 45. P. 3986;
Glück M., Reya E., Vogt A. // Ibid. V. 46. P. 1973.
69. *Aurenche P., Guillet J. P., Fontanaz M.* // Z. Phys. C. 1994. V. 64. P. 621.
70. *Lai H. L. et al.* (*CTEQ Collab.*) // Eur. Phys. J. C. 2000. V. 12. P. 375.
71. *Martin A. D. et al.* // Ibid. V. 14. P. 133.
72. *Bethke S.* // J. Phys. G. 2000. V. 26. P. R27;
Bethke S. hep-ex/0211012.
73. *Breitweg J. et al.* (*ZEUS Collab.*) // Phys. Lett. B. 2001. V. 507. P. 70;
Chekanov S. et al. (*ZEUS Collab.*) // Phys. Lett. B. 2002. V. 547. P. 164.
74. *Adloff C. et al.* (*H1 Collab.*) // Eur. Phys. J. C. 2001. V. 19. P. 289.
75. *Affolder T. et al.* (*CDF Collab.*) // Phys. Rev. Lett. 2002. V. 88. P. 042001.
76. *Derrick M. et al.* (*ZEUS Collab.*) // Phys. Lett. B. 1995. V. 348. P. 665.
77. *Adloff C. et al.* (*H1 Collab.*) // Eur. Phys. J. C. 2002. V. 25. P. 13.
78. *Chekanov S. et al.* (*ZEUS Collab.*) // Ibid. V. 23. P. 615.
79. *Breitweg J. et al.* (*ZEUS Collab.*) // Eur. Phys. J. C. 1999. V. 11. P. 35.
80. *Marchesini G., Webber B. R.* // Nucl. Phys. B. 1984. V. 238. P. 1;
Webber B. R. // Ibid. P. 492;
Marchesini G., Webber B. R. // Nucl. Phys. B. 1988. V. 310. P. 461;
Marchesini G. et al. // Comp. Phys. Commun. 1992. V. 67. P. 465;
Marchesini G. et al. HERWIG 5.9. hep-ph/9607393.

81. *Frixione S., Ridolfi G.* // Nucl. Phys. B. 1997. V. 507. P. 4007;
Frixione S. // Ibid. P. 295.

82. *Chekanov S. et al.* (*ZEUS Collab.*) // Eur. Phys. J. C. 2002. V. 27. P. 173.

83. *Abe F. et al.* (*CDF Collab.*) // Phys. Rev. Lett. 1997. V. 79. P. 572;
Abe F. et al. (*CDF Collab.*) // Ibid. P. 578.

84. *Krämer M. et al.* // Phys. Lett. B. 1995. V. 348. P. 657;
Krämer M. et al. // Nucl. Phys. B. 1996. V. 459. P. 3;
Krämer M. // Prog. Part. Nucl. Phys. 2001. V. 47. P. 141.

85. *Kniehl B. A., Kramer G.* // Eur. Phys. J. C. 1999. V. 6. P. 493.

86. *ZEUS Collab.* Contribution // XXXI Intern. Conf. on High Energy Physics, Amsterdam, July 24–31, 2002. Abstr. 785.

87. *Frixione S. et al.* // Phys. Lett. B. 1995. V. 348. P. 633.

88. *Adloff C. et al.* (*H1 Collab.*) // Phys. Lett. B. 1999. V. 467. P. 156;
Breitweg J. et al. (*ZEUS Collab.)* // Eur. Phys. J. C. 2001. V. 18. P. 625;
H1 Collab. Contribution // XXX Intern. Conf. on High Energy Physics, Budapest, July 12–18, 2001. Abstr. 807.

89. *ZEUS Collab.* Contribution // XXXI Intern. Conf. on High Energy Physics, Amsterdam, July 24–31, 2002. Abstr. 784.